Dynamical Properties and Chaos of the Multicellular Converter Associated With a Nonlinear Load

Philippe Djondiné, Jean-Pierre Barbot

ISSN (Print) : 2320 – 3765
ISSN (Online): 2278 – 8875

International Journal of Advanced Research in Electrical, Electronics and Instrumentation Engineering

(A High Impact Factor, Monthly, Peer Reviewed Journal)

Website: www.ijareeie.com

Vol. 6, Issue 11, November 2017

Dynamical Properties and Chaos of the Multicellular Converter Associated With a Nonlinear Load

Philippe Djondiné[1,2], Jean-Pierre Barbot[2]

Department of Physics, Faculty of science, the University of Ngaoundéré, Cameroon [1]

ECS-Lab, EA3649, ENSEA, Cergy Cedex, Cergy-Pontoise 95014, France, Quartz EA 7393[2]

ABSTRACT: The multicellular chopper connected with a nonlinear load is investigated by detailed theoretical and analysis as well as dynamic simulation, including some basic dynamical properties, Lyapunov exponent, fractal dimension, bifurcation diagrams and routes to chaos. In the parameter space where the equilibria of the system are both asymptotically stable, chaotic attractors coexist with period attractors and stable equilibria. Our system displays 2 scroll chaotic attractors for certain values of its parameters.

KEYWORDS: chaotic attractors, chaos, equilibria and stability, Lyapunov exponent, multicellular converter.

I.INTRODUCTION

The power electronics knows important technological developments. This is carried out thanks to the developments of the semiconductor of power components but also of new systems of energy conversion. Among these systems, multicellular converters are based on the association in series of the elementary cells of commutation. This structure appeared at the beginning of the 90's [1], makes it possible to share the constraints in tension and/or while running in high voltages installations by the cells of commutation series-connected and also to improve the harmonic contents of the forms of waves. To benefit as well as possible from the large potential of the multicellular structure, research then went in various directions. Initially models were developed to describe their instantaneous behaviors [2], harmonic [3] or averaging [4] and [5]. These various models were used at the base for the development of laws of open-loop control [6] and closed-loop [7]. Modeling is a very important phase for the synthesis of the laws of order.
In recent decades, it was discovered that most of static converters were the seat of unknown nonlinear phenomena in power electronics [8 – 11]**.** It is for example the case of multicellular choppers that can exhibit unusual and sometimes chaotic behaviors. Obviously this may generate dramatical consequences. There have been many methods for detecting chaos from order [12]. They include Poincaré sections, Lyapunov exponents [13], fast Lyapunov indicators [14], Smaller Alignment Index (SALI) [15] and its generalized alignment index [16], bifurcations, power spectra [17], frequency analysis [18], 0-1 test [19], geometrical criteria [20, 21], fractal basin boundaries [22], etc. Each of them has its advantages and drawbacks in classifying the attractors. Here, we investigate the level of chaos in our system through numerical simulations by means of computing the Lyapunov Exponents, bifurcation diagram, first return map to the Poincaré section, and the phase diagram.
In this article, we study the dynamical properties of a two cells chopper connected to nonlinear load. For that, the instantaneous model of the two-cell chopper is considered. The paper is organized as follows: In the first section, some definitions and notation used for instantaneous model of p-cell chopper are introduced. Basic dynamical properties of a two cells chopper connected to nonlinear load are also investigated in section 3. Finally, chaotic behavior and simulation results are presented in section 4.

II.P-CELL CONVERTER MODEL

Throughout the paper, the p-cell converter connects in series p elementary cells and a passive load R and L as illustrated in figure 1. Each switching cell is controlled by a binary input signal $u_k(t)$ for $k = 1 \dots p$. This signal $u_k(t)$

ISSN (Print) : 2320 – 3765
ISSN (Online): 2278 – 8875

International Journal of Advanced Research in Electrical, Electronics and Instrumentation Engineering

(A High Impact Factor, Monthly, Peer Reviewed Journal)

Website: www.ijareeie.com

Vol. 6, Issue 11, November 2017

is equal to 1 when the upper switch of the cell is conducting and 0 when the lower complementary switch of the cell is conducting. In order to ensure that, we must determine the floating capacitor voltages:

$$V_{cellk} = V_{C_k} - V_{C_{k-1}} = k\frac{E}{p}\ ; \quad k = 1 \dots \dots p \qquad (1)$$

where $V_{C_0} = 0\ ;\ V_{C_p} = E$,

From equation. (1), for $k = 1$, we have:

$$V_{cell1} = V_{C_1} - V_{C_0} = \frac{E}{p} \Rightarrow V_{C_1} = \frac{E}{p} \qquad (2)$$

Increasing k, we find the general expression for the capacitor voltages:

$$V_{C_k} = k\frac{E}{p} \qquad (3)$$

In order to determine the converter model, we consider two adjacent cells: $cell_k$ and $cell_{k+1}$ connected with the capacitor C_k (Figure 1). The capacitor voltage V_{C_k} is determined by the evolution of the capacitor current. This, in turn, is given by the configuration of the switches:

$$i_{C_k} = (u_{k+1} - u_k)i_L \qquad (4)$$

where $u_k = 1$ if the upper switch in $cell_k$ is conducting and $u_k = 0$ if the lower switch in $cell_k$ is conducting. The capacitor voltage is then given by equation (5):

$$i_{C_k} = C_k\frac{dV_{C_k}}{dt} \Rightarrow \frac{dV_{C_k}}{dt} = \frac{u_{k+1} - u_k}{C_k}.i_L \qquad (5)$$

Equation (5) can be generalized for all capacitors. Next we determine the output voltage as the sum of all cell voltages:

$$V_s = \sum_{k=1}^{p} V_{cell_k} = \sum_{k=1}^{p}(V_{C_k} - V_{C_{k-1}})i_L \qquad (6)$$

From equation (6), we note that we can have multiple voltage levels at the output, depending on the configuration of the switches. For a converter with p cells, we have $p + 1$ voltage levels: $0, \frac{E}{p}, \frac{2E}{p}, \dots, \frac{(p+1)E}{p}, E$. This means that the voltage jumps at the output are smaller than the ones in classical structures. For the multicell converter with an RL load in figure 1, the output current i_L is given by:

$$\frac{di_L}{dt} = \frac{V_s}{L} - \frac{R}{L}i_L \qquad (7)$$

From equations. (5), (6) and (7) we get the instantaneous model of the multicell converter in figure 2:

$$\begin{cases} \frac{di_L}{dt} = \frac{u_2 - u_1}{L}V_{C_1} + \frac{u_3 - u_2}{L}V_{C_2} + \dots + \frac{u_p - u_{p-1}}{L}V_{C_{p-1}} + \frac{u_p}{L}E - \frac{R}{L}i_L \\ \frac{dV_{C_1}}{dt} = \frac{u_2 - u_1}{C_1}i_L \\ \frac{dV_{C_2}}{dt} = \frac{u_3 - u_2}{C_2}i_L \\ \quad . \\ \quad . \\ \quad . \\ \frac{dV_{C_{p-1}}}{dt} = \frac{u_p - u_{p-1}}{C_{p-1}}i_L \end{cases} \qquad (8)$$

ISSN (Print) : 2320 – 3765
ISSN (Online): 2278 – 8875

International Journal of Advanced Research in Electrical, Electronics and Instrumentation Engineering

(A High Impact Factor, Monthly, Peer Reviewed Journal)

Website: www.ijareeie.com

Vol. 6, Issue 11, November 2017

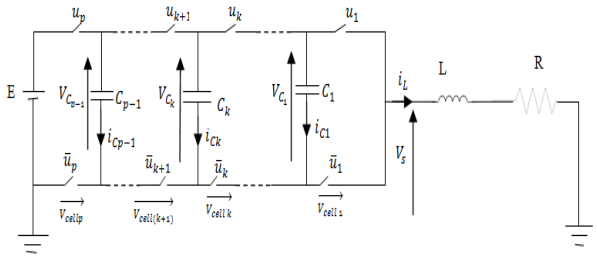

Figure 1: A p cells converter connected to RL load

where V_{C_k} is the k^{th} flying capacitor voltage and i_L is the output load current, which is the only measurable output. C_k for $k = 1 \ldots p$; are the capacitors, E is the voltage of the source, R is the resistance and L is the inductance.

III.TWO CELLS MULTICELLULAR AND METHODS TO QUANTIFY THEIR BEHAVIORS

The two-cells multicellular chopper (figure 2) system is described as:

$$\begin{cases} L\dfrac{di_L}{dt} = (u_2 - u_1).v_C - v_{C_l} - R.i_L + u_2.E \\ C\dfrac{dv_C}{dt} = (u_2 - u_1).i_L \\ C_l\dfrac{dv_{C_l}}{dt} = i_L - g(v_{C_l}) \end{cases} \quad (9)$$

where $g(.)$ is a piecewise – linear function

$$g(v_{C_l}) = G_b v_{C_l} + 0.5.(G_a - G_b)\left(|v_{C_l} + B_p| - |v_{C_l} - B_p|\right) \quad (10)$$

which is the mathematical representation of the characteristic curve of nonlinear load. The slopes of the inner and outer regions are G_a and G_b, while B_p indicates break points. Rescaling equation (2) as $v_C = x_2 B_p$, $v_{C_l} = x_3 B_p$, $i_L = x_1 G B_p$, $G = \frac{1}{R}$, $t = \frac{C}{G}\tau$ and then redefining τ as t the following set of normalized equations are obtained:

$$\begin{cases} \dot{x}_1 = \beta(\varepsilon x_2 - x_3 - \gamma x_1) + \alpha u_2 \\ \dot{x}_2 = \varepsilon x_1 \\ \dot{x}_3 = p(x_1 - g(x_3)) \end{cases} \quad (11)$$

where $\varepsilon = u_2 - u_1$, $p = \frac{C}{C_l}, \beta = \frac{C}{LG^2}, \gamma = RG, \alpha = \frac{\beta E}{B_p}$

Obviously $g(x_3) = bx_3 + 0.5(a-b)[|x_3 + 1| - |x_3 - 1|]$, or

$$g(x_3) = \begin{cases} bx_3 + a - b, & x_3 > 1 \\ ax_3, & |x_3| \le 1 \\ bx_3 - a + b, & x_3 < -1 \end{cases} \quad (12)$$

here $a = \frac{G_a}{G}$, $b = \frac{G_b}{G}$.

ISSN (Print) : 2320 – 3765
ISSN (Online): 2278 – 8875

International Journal of Advanced Research in Electrical, Electronics and Instrumentation Engineering

(A High Impact Factor, Monthly, Peer Reviewed Journal)

Website: www.ijareeie.com

Vol. 6, Issue 11, November 2017

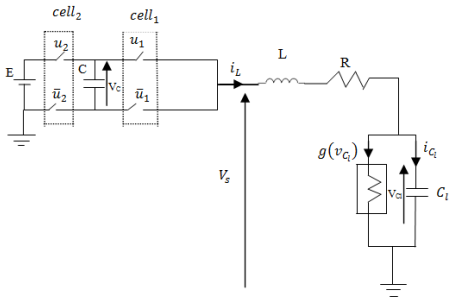

Figure 2: Two cells chopper connected to a nonlinear load

Its function is to supply a passive load (RL) in series with another nonlinear load connected in parallel with a capacitor [23]. Four operating modes are then possible as shown in figure 3. Note that the floating source takes part in the evolution of the dynamics of the system only to the third and fourth mode. In the third mode, the capacity discharges and charge during the fourth mode. Thus, if these two modes last same time with a constant charging current, then the average power transmitted by this floating source over one period of commutation is null. We also notice that these two modes make it possible to obtain by commutation the additional level $\frac{E}{2}$ on the output voltage V_s. As the switches of each cell are regarded as ideals, their behavior can be to model by a discrete state taking of the values $0\,(on)$ or $1\,(off)$. In practice, some of these states never will be visited for reasons of safety measures or following the strategy of order adopted or because of the structure of the converter him finally to even or comply with the rule of adjacency. The transitions are not necessarily controlled

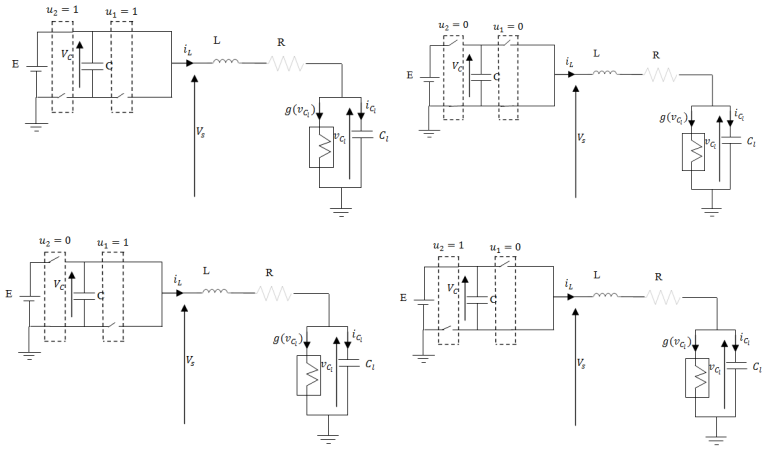

Figure 3: Switching cell and its configurations.

Some important basic features of this system are:

1. It is autonomous, which means that time does not explicitly appear on the right hand side.

2. The equations involve only first order time derivatives, so the evolution depends only on the values of x_1, x_2, and x_3 at the time.

3. Due to the piecewise-linear function in the third equation, the system is non-linear.

4. The system is dissipative when the following inequality holds:

$$\nabla V = \frac{\partial \dot{x}_1}{\partial x_1} + \frac{\partial \dot{x}_2}{\partial x_2} + \frac{\partial \dot{x}_3}{\partial x_3} = \begin{cases} -\beta\gamma - pb, & |x_3| > 1 \\ -\beta\gamma - pa, & |x_3| \leq 1 \end{cases} \quad (13)$$

Since parameters β, γ, p, b and a, denoting the physical characteristics of the air flow, are positive, the inequality always holds and, thus, solutions are bounded and, thus, solutions are bounded.

5. The system is symmetric, with respect to the x_2 axis, which means it is invariant for the coordinate transformation: $(x_1, x_2, x_3) \rightarrow (x_1, -x_2, x_3)$

ISSN (Print) : 2320 – 3765
ISSN (Online): 2278 – 8875

International Journal of Advanced Research in Electrical, Electronics and Instrumentation Engineering

(A High Impact Factor, Monthly, Peer Reviewed Journal)

Website: www.ijareeie.com

Vol. 6, Issue 11, November 2017

Chaos is described as the irregular, unpredictable behavior of deterministic, non-linear dynamical systems. In order to have chaotic behavior, simultaneous stretching and folding in the dynamics of the system are essential [24, 25]. Stretching ensures the sensitivity to initial conditions and folding guarantees that the attractor is bounded. Stretching and folding are equivalent to positive and negative Lyapunov Exponents, respectively. Therefore, in chaotic dynamics, stretching in one direction is observed by the existence of one positive Lyapunov Exponent in that direction [26]. Using the method reported by Wolf et al. [27], the corresponding Lyapunov exponent of the real multicellular chopper connected with a nonlinear load system is computed by fixing $p = 25.10^{-4}$, $\alpha = 2.10^{-2}$, $a = -15$, $b = 5$, $\gamma = 1$ and varying β, as the control parameter. The initial conditions in all these simulations are the same and are equal to $(x_{10}, x_{20}, x_{30}) = [0, 5, 4]$.

According to the detailed numerical as well as theoretical analysis and (13), the Lyapunov exponents are found to be:

- For $\varepsilon = \pm 1$, $l_{E1} = 0.0318$, $l_{E2} = -0.0319$, $l_{E3} = -0.0128$

Therefore, the Lyapunov dimension of this system is:

$$D_L = j + \frac{\sum_{i=1}^{j} l_i}{|l_{j+1}|} = 2 + \frac{0.0318 - 0.0319}{|-0.0128|} = 2.0078125 \qquad (14)$$

- For $\varepsilon = 0$, $l_{E1} = -1.4029.10^{-4}$, $l_{E2} = 0$, $l_{E3} = -0.0126$

Therefore, the Lyapunov dimension of this system is:

$$D_L = j + \frac{\sum_{i=1}^{j} l_i}{|l_{j+1}|} = 2 + \frac{-1.4029.10^{-4}}{|-0.0126|} = 1.98886587 \qquad (15)$$

Equation (14) and (15) means system (11) is really a dissipative system, and the Lyapunov dimensions of the system are fractional. Having a strange attractor and positive Lyapunov exponent, it is obvious that the system is really a 3D chaotic system. The null Lyapunov exponent is obviously related to the critical nature between expansion and contracting nature of different directions in phase space.

In addition, the bifurcation diagram was plotted for our systems, which is the most useful graphical representation of the sequence of bifurcations that take place in the system when the control parameter changes. The bifurcation diagrams of the state variable x_1 in system (11) are shown in figure

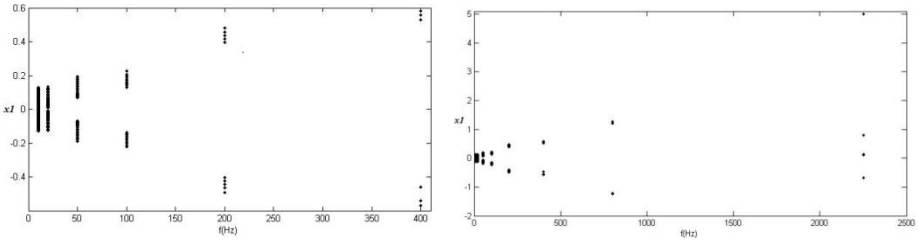

Figure 4: Bifurcation diagrams

The first return map to the Poincaré section (figure 5) is a common tool for analyzing the existence and stability of periodic trajectories of dynamical systems. It is defined on a hyper-surface formed by a Poincaré section (figure 6), which is transverse to the trajectory of the system [28]. In this study, these maps were formed by plotting the local maxima of the variable x_3, and the real part of the variable.

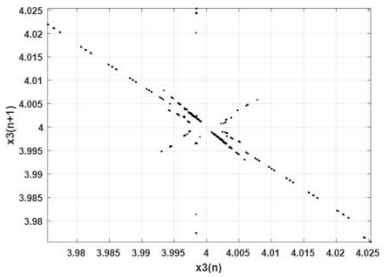

Figure 5: First return map

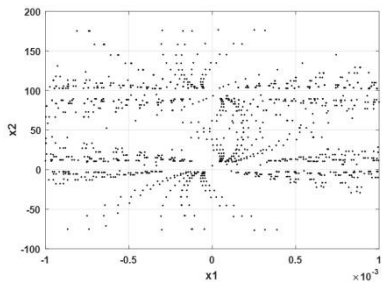

Figure 6: The Poincaré section of $x_1 - x_2$ plane

ISSN (Print) : 2320 – 3765
ISSN (Online): 2278 – 8875

International Journal of Advanced Research in Electrical, Electronics and Instrumentation Engineering

(A High Impact Factor, Monthly, Peer Reviewed Journal)

Website: www.ijareeie.com

Vol. 6, Issue 11, November 2017

IV.DYNAMICAL ANALYSIS OF THE TWO-CELLS MULTICELLULAR CHOPPER ASSOCIATED WITH A NONLINEAR LOAD

- Equilibria

The equilibria of (4) can be calculated by solving the following algebraic equations simultaneously

$$\begin{cases} \dot{x}_1 = \beta(\varepsilon x_2 - x_3 - \gamma x_1) + \alpha u_2 = 0 \\ \dot{x}_2 = \varepsilon x_1 = 0 \\ \dot{x}_3 = p(x_1 - g(x_3)) = 0 \end{cases}$$

Case 1. $\boldsymbol{\varepsilon = 1}$**, i.e.,** $\boldsymbol{u_1 = 0, u_2 = 1}$

i. $x_3 > 1$, the equilibrium point is : $E_1 = \begin{pmatrix} 0 \\ \frac{b-a}{b} - \frac{\alpha}{\beta} \\ \frac{b-a}{b} \end{pmatrix}$

ii. $|x_3| \leq 1$, the equilibrium point is : $E_2 = \begin{pmatrix} 0 \\ -\frac{\alpha}{\beta} \\ 0 \end{pmatrix}$

iii. $x_3 < -1$, the equilibrium point is : $E_3 = \begin{pmatrix} 0 \\ \frac{a-b}{b} - \frac{\alpha}{\beta} \\ \frac{a-b}{b} \end{pmatrix}$

Case 2. $\boldsymbol{\varepsilon = -1}$**, i.e.,** $\boldsymbol{u_1 = 1, u_2 = 0}$

i. $x_3 > 1$, the equilibrium point is : $E_{11} = \begin{pmatrix} 0 \\ \frac{a-b}{b} \\ \frac{-a+b}{b} \end{pmatrix}$

ii. $|x_3| \leq 1$, the equilibrium point is : $E_{21} = \begin{pmatrix} 0 \\ 0 \\ 0 \end{pmatrix}$

iii. $x_3 < -1$, the equilibrium point is : $E_{31} = \begin{pmatrix} 0 \\ \frac{-a+b}{b} \\ \frac{a-b}{b} \end{pmatrix}$

Case 3 : $\boldsymbol{\varepsilon = 0}$

a) $\boldsymbol{u_2 = u_1 = 1}$

i. $x_3 > 1$; the equilibrium point is : $E_{12} = \begin{pmatrix} \frac{a+\left(\frac{\alpha}{\beta}-1\right)b}{1+b\gamma} \\ x_2 \\ \frac{\gamma(-a+b)+\frac{\alpha}{\beta}}{1+b\gamma} \end{pmatrix}$

ii. $|x_3| \leq 1$; we obtain: $E_{22} = \begin{pmatrix} \frac{a\frac{\alpha}{\beta}}{1+a\gamma} \\ x_2 \\ \frac{\frac{\alpha}{\beta}}{1+a\gamma} \end{pmatrix}$

iii. $x_3 < -1$; we obtain : $E_{32} = \begin{pmatrix} \frac{-a+\left(1+\frac{\alpha}{\beta}\right)b}{1+b\gamma} \\ x_2 \\ \frac{\gamma(a-b)+\frac{\alpha}{\beta}}{1+b\gamma} \end{pmatrix}$

ISSN (Print) : 2320 – 3765
ISSN (Online): 2278 – 8875

International Journal of Advanced Research in Electrical, Electronics and Instrumentation Engineering

(A High Impact Factor, Monthly, Peer Reviewed Journal)

Website: www.ijareeie.com

Vol. 6, Issue 11, November 2017

b) $u_1 = u_2 = 0$

i. $x_3 > 1$; the equilibrium point is : $E_{13} = \begin{pmatrix} \frac{a-b}{1+b\gamma} \\ x_2 \\ \frac{-\gamma(a-b)}{1+b\gamma} \end{pmatrix}$

ii. $|x_3| \leq 1$; the equilibrium point is: $E_{23} = \begin{pmatrix} 0 \\ x_2 \\ 0 \end{pmatrix}$.

iii. $x_3 < -1$; the equilibrium point is: $E_{33} = \begin{pmatrix} \frac{-a+b}{1+b\gamma} \\ x_2 \\ \frac{-\gamma(-a+b)}{1+b\gamma} \end{pmatrix}$

- Stability

Let us study the stability of different equilibrium points.

1. **For** $|x_3| > 1$, the Jacobian matrix is defined as $J = \begin{bmatrix} -\beta\gamma & \beta\varepsilon & -\beta \\ \varepsilon & 0 & 0 \\ p & 0 & -bp \end{bmatrix}$

The eigenvalues are:

i. **If** $= \pm 1$; $\lambda_1 = 0.0140$; $\lambda_2 = -0.0141$; $\lambda_3 = -0.0126$; here λ_1 is a positive real number, λ_2 and λ_3 are two negatives real numbers. Therefore, the equilibrium E_1 *and* E_{11} are a saddle point in the plane (x_1, x_2) and (x_1, x_3); these equilibrium are unstable.

ii. **If** $\boldsymbol{\varepsilon = 0}$ **;** $\lambda_1 = -0.0002$; $\lambda_2 = -0.0125$; $\lambda_3 = 0$; Then E_{12} *and* E_{13}, are stable equilibrium points within the meaning of Lyapunov for all x_2.

2. **For** $|x_3| \leq 1$, the Jacobian matrix is defined as $J = \begin{bmatrix} -\beta\gamma & \beta\varepsilon & -\beta \\ \varepsilon & 0 & 0 \\ p & 0 & -pa \end{bmatrix}$

Three characteristic values of the Jacobian matrix J can be obtained from $|\lambda I - J| = 0$ as follows:

i. **If** $= \pm 1$; $\lambda_1 = 0.0140$; $\lambda_2 = -0.0143$; $\lambda_3 = -0.0375$; here λ_1 is a positive real number, λ_2 and λ_3 are two negative real numbers. Therefore, the equilibrium E_2 *and* E_{21} are a saddle foci in the plane (x_1, x_2) and (x_1, x_3); these equilibrium are unstable.

ii. **If** $\boldsymbol{\varepsilon = 0}$ **;** $\lambda_1 = -0.0002$; $\lambda_2 = -0.0375$; $\lambda_3 = 0$; E_{23} is a stable equilibrium point within the meaning of Lyapunov for all x_2.

3. **For** $|x_3| < -1$, the Jacobian matrix is defined as $J = \begin{bmatrix} -\beta\gamma & \beta\varepsilon & -\beta \\ \varepsilon & 0 & 0 \\ p & 0 & -bp \end{bmatrix}$

The eigenvalues are:

i. **If** $= \pm 1$; $\lambda_1 = 0.0140$; $\lambda_2 = -0.0141$; $\lambda_3 = -0.0126$; here λ_1 is a positive real number, λ_2 and λ_3 are two negatives real numbers. Therefore, the equilibrium E_3 *and* E_{31} are a saddle point in the plane(x_1, x_2) and (x_1, x_3); these equilibrium are unstable.

ii. **If** $\boldsymbol{\varepsilon = 0}$ **;** $\lambda_1 = -0.0002$; $\lambda_2 = -0.0125$; $\lambda_3 = 0$; then E_{12} *and* E_{13}, are stable equilibrium points within the meaning of Lyapunov for all x_2.

Regarding the figure 4, it is obvious that this system is chaotic for small ranges of parameter f.

The behaviors of system (11) changes for different values of parameter β. Figure 7 demonstrate some phase portraits of system (11) for some of these values when the behaviors are periodic, quasi-periodic, chaotic or hyper-chaotic.

ISSN (Print) : 2320 – 3765
ISSN (Online): 2278 – 8875

International Journal of Advanced Research in Electrical, Electronics and Instrumentation Engineering

(A High Impact Factor, Monthly, Peer Reviewed Journal)

Website: www.ijareeie.com

Vol. 6, Issue 11, November 2017

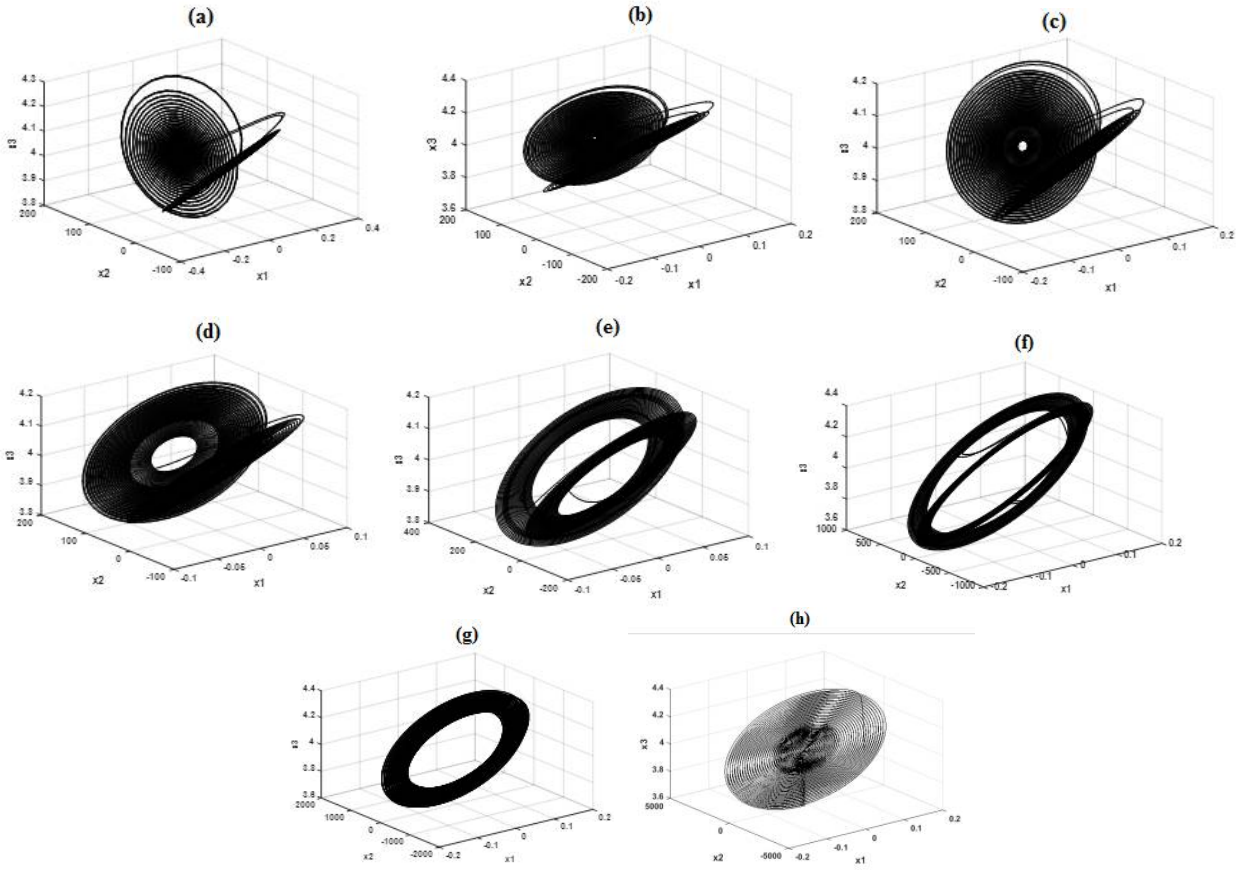

Figure 7: Phase portraits: **(a)** $\beta = 5.10^{-4}, L = 0.02H$; **(b):** $\beta = 2{,}5.10^{-4}, L = 0.04H$; **(c):** $\beta = 2.10^{-4}, L = 0.05H$; **(d):** $\beta = 10^{-4}, L = 0.1H$; **(e):** $\beta = 0{,}2.10^{-4}, L = 0.5H$; **(f):** $\beta = 10^{-5}, L = 1H$; **(g):** $\beta = 10^{-6}, L = 10H$; **(h):** $\beta = 10^{-7}, L = 100H$

V. CONCLUSION

This paper explains the dynamics of the multicellular chopper connected with a nonlinear load. This system is autonomous, non-linear, dissipative with bounded solutions, symmetric with respect to the x_2 axis, and they involve only first order time derivatives. The phase portraits, Lyapunov Exponents, bifurcation diagrams, first return maps to the Poincare sections and Poincaré section of the system prove that it is possible to have chaos in the system expressed. Indeed, the steady state trajectory of this system can be attracted to a limit cycle, a torus, a chaotic attractor as shown in figure 7.

REFERENCES

[1] T.A. Meynard and H. Foch. Brevet français No. 91.09582 du 25 juillet 91, dépôt International PCT (Europe, Japon, USA, Canada) No. 92/00652 du 8 Juillet 92, 1991.
[2] A. Donzel. Commande des convertisseurs multiniveaux : Application à un moteur asynchrone Thèse de doctorat, Institut National Polytechnique de Grenoble 2000
[3] M. Fadel and T.A. Meynard. Equilibrage des tensions dans les convertisseurs statiques multicellulaires série: Modélisation EPF Grenoble, pp. 115-120, 1996.
[4] R. Bensaid, R., and M. Fadel. (2001). Sliding modes observer for multicell converters. In NOLCOS, 2001.
[5] R. Stala, S. Pirog, A. Mondzik, M. Baszynski, A. Penczek, J. Czekonski and S. Gasiorek, "Results of investigation of multicell converters with balancing circuit," *IEEE Trans. Industrial Electronics*, vol. 56, no. 7, pp. 2620–2628, July 2009.

ISSN (Print) : 2320 – 3765
ISSN (Online): 2278 – 8875

International Journal of Advanced Research in Electrical, Electronics and Instrumentation Engineering

(A High Impact Factor, Monthly, Peer Reviewed Journal)

Website: www.ijareeie.com

Vol. 6, Issue 11, November 2017

[6] O. Tachon, M. Fadel and T. Meynard., "Control of series multicell converters by linear state feedback decoupling" EPF Grenoble, pp. 1588-1593, 1997.
[7] Bethoux, O. Barbot, J.-P. Multi-cell chopper direct control law preserving optimal limit cycles. In IEEE CCA, 2002.
[8] M. Di Bernardo and K. Tse Chi. Bifurcation and chaos in power electronics : an overview in nonlinear dynamics in engineering. Edited by Prof. G. Chen, 2002.
[9] F. Defay, A. M. Llor, and M. Fadel. A predictive control with flying capacitor balancing of a multicell active power filter. IEEE Trans. On Industrial Electronics, 55(9):3212–3220, 2008.
[10] J. I. Leon, R. Portillo, S. Vazquez, and J. J. Padilla. Simple unified approach to develop a time-domain modulation strategy for singlephase multilevel choppers. IEEE Trans. on Industrial Electronics, 55(9):3239–3248, 2008.
[11] M. Di Bernardo and K. Tse Chi. Chaos in power electronics : An overview. Chaos in Circuits and Systems, pages 317 – 340, 2002.
[12] G. Contopoulos, Order and Chaos in Dynamical Astronomy, Springer Verlag, Berlin, 2002
[13] G. Benettin, L. Galgani, J. M. Strelcyn, Kolmogorov entropy and numerical experiments, Phys. Rev. A, 14, 1976, 2338-2445
[14] C. Froeschlé, E. Lega, R. Gonczi, Fast Lyapunov indicators. Applications to asteroidal motion, Celest. Mech. Dyn. Astron., 67, 1997, 41-62
[15] C. Skokos, Alignment indices: A new, simple method for determining the ordered or chaotic nature of orbits, J. Phys. A, 34, 2001, 10029-10043
[16] C. Skokos, T. Bountis, C. Antonopoulos, Geometrical properties of local dynamics in Hamiltonian systems: The Generalized Alignment Index (GALI) method, Physica D, 231, 2007, 30-54
[17] J. Binney, D. Spergel, Spectral stellar dynamics, Astrophys. J., Vol. 252, 1982, 308-321
[18] J. Laskar, The chaotic motion of the solar system: A numerical estimate of the size of the chaotic zones, Icarus 88(2), 1990, 266-291
[19] G. A. Gottwald, I. Melbourne, A new test for chaos in deterministic systems, Proc. R. Soc. London, Ser. A, 460 (2042), 2004, 603-611
[20] L. Horwitz, Y. B. Zion, M. Lewkowicz, M. Schiffer, J. Levitan, Geometry of Hamiltonian chaos, Phys. Rev. Lett., 98, 2007, 234301
[21] X. Wu, Is the Hamiltonian geometrical criterion for chaos always reliable? Journal of Geometry and Physics, 59, 2009, 1357-1362
[22] J. Levin, Gravity waves, chaos, and spinning compact binaries, Phys. Rev. Lett., 84, 2000, 3515
[23] P. Djondiné, M. Ghanes, J-P. Barbot, and B. Essimbi Dynamical behaviors of multicellular chopper. Journal of Control Science and Engineering, 2(1), 35–42, (2014).
[24] J.M. Ottino, ''The kinematics of mixing: stretching, chaos, and transport'', In Cambridge Texts in Applied Mathematics, Cambridge University Press, Cambridge, UK (1989).
[25] A. Tufaile, and A.P.B. Tufaile, ''Stretching and folding mechanism in foams'', Phys. Lett. A, 372(42), pp. 6381–6385 (2008).
[26] E.D. Ubeyli, and I. Guler, ''Statistics over Lyapunov exponents for feature extraction: electroencephalographic changes detection case'', World Acad. Sci. Eng. Tech., 2, pp. 132–135 (2005).
[27] A. Wolf, J. B. Swift, H. L. Swinney, and J. A. Vastano, ''Determining Lyapunov exponents from a time series'', Physica D, 16(3), pp. 285–317 (1985).
[28] P. Djondiné, R. He, M. Ghanes and J-P. Barbot, Chaotic behavior study for serial multicellular chopper connected to nonlinear load; Proceedings of the 3rd International Conference on Systems and Control, Algiers, Algeria, October 29-31, 2013